Electromagnetic Simulations of Microwave Trapping Structures

A thesis submitted in partial fulfillment of the requirement
for the degree of Bachelor of Arts/ Science in
Physics from William and Mary

by

Chloe Lewelling

Advisor: Seth Aubin
Senior Research Coordinator: Irina Novikova

Williamsburg, Virginia
May 2018

Contents

Acknowledgments

I want to thank thank Seth Aubin for designing the geometries tested, teaching me the science behind the geometries, and advising me throughout my research.

I would also like to thank Andrew Rotunno for showing me how to use Cadfeko and Shuangli Du for showing me how to create a Faraday cage in Cadfeko.

List of Figures

List of Tables

Abstract

Electromagnetic near fields can be used to trap and manipulate ultracold atoms and small dielectric particles. Atom chips are used to generate micro-magnetic traps produced by DC currents for ultracold atoms, and this work investigates the possibility of using microwave near fields for similar manipulation of such atoms. Furthermore, microwave near fields may also be used as "tweezers" for precise control of the movement of small dielectric particles. Using FEKO, a commercial electromagnetic simulation software, several geometries were simulated with a microwave frequency to find new electric field maximums and minimums that can be used for tweezer and atom chip applications.

The "two strand trap" and "three strand trap" simulations created local electric field minimums in their center. The "microwave lattice" simulation shows that the position of an electric field minimum can be controlled. A 3D simulation of two parallel disks created an electric field maximum in the xy-plane between them. A configuration consisting of two semi-spheres acting like a capacitor created a local microwave electric field maximum in all three directions. A planar configuration created a local electric field maximum above the configuration.

Chapter 1

Introduction

1.1 Objective

The objective of this research is to model the electromagnetic fields of various microstrip configurations and 3D structures with a frequency in the microwave range in order to test their potential for future ultracold atom and microsphere trapping.

1.2 Ultracold Atoms

At William and Mary, the Ultra-Cold atom group created an optical dipole trap that uses a focused laser beam to constrain ultracold atoms as seen in figure 1.1. [9]. Focused laser beams have also been used to create optical tweezers, trapping and manipulating dielectric microspheres that are suspended in a dielectric liquid.

Atom chips, as shown in figure 1.1, use DC currents to create magnetic field minimums that trap weak field seeking states. This thesis investigates whether microwave near fields can be used on atoms chips to create traps for ultracold atoms.

1.3 Microspheres

Microwave near fields, created by the atom chip, also have the potential to trap dielectric microspheres suspended in a dielectric liquid. Earnshaw′s theorem

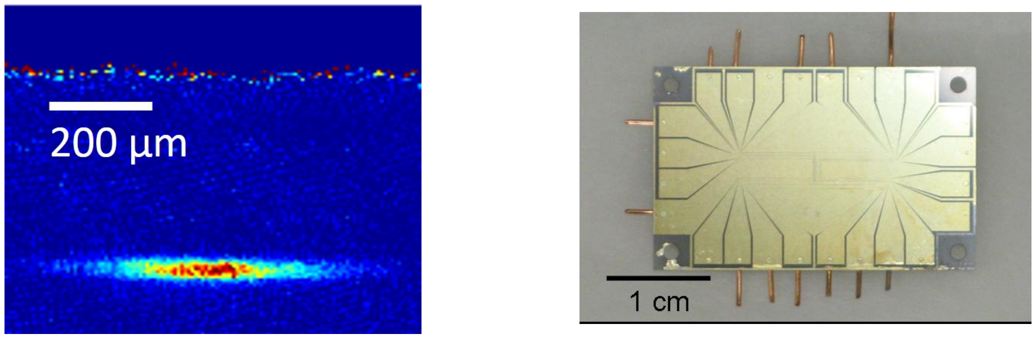

Figure 1.1: The left image shows a focused laser beam was used to created a Atom Trap for ultracold ^{87}R by the Ultra-Cold Physics Group (Dept. of Physics, William and Mary). The right image is an atom chip used in the Ultracold Matter Group (Dept. of Physics, William and Mary) from Thywissen group (Dept. of Physics, University of Toronto) [9]

states that there are no local maxima for electrostatic and magnetostatic fields. A electromagnetic wave in the far-field can have a local maximum, such as in figure 1.1, where a local maximum was created using a focused laser. This thesis investigates whether the time-dependence of microwaves can be used as a loophole in creating local field maxima.

Dielectric microspheres can be used in place of atoms in a large scale model of atoms traps. Unlike atoms, which can be trapped by the magnetic field, dielectric microspheres are trapped and manipulated by the electric field. However, in many propagating electromagnetic fields, local electric field minimums will correspond to local magnetic field minimums, with a few exceptions such as in the electionmagnetic field created by standing waves. Therefore, if a large-scale microchip is submerged in a dielectric liquid traps microspheres, then a smaller atom chip with the same configuration will trap atoms.

1.4 Structure of Thesis

This thesis is structured in the following manner. Section 2 of this thesis introduces the physics of microstrips, the behavior of a dielectric microspheres, and the simulation software FEKO. In addition, this sections also discusses the physics behind each of the models. Section 3 covers the models that produce an electromagnetic field minimum. Section 4 covers the models that produce an electric field maximum.

Chapter 2

Theory

2.1 Dielectric Theory

Dielectric microspheres submerged in a dielectric liquid act as high field seekers or low fields seekers, depending on their dielectric constant. This property of dielectric microspheres is a result of their dipole moment. The dipole moment of a dielectric sphere suspended in a dielectric liquid is:[8]

$$\vec{p} = 4\pi r^3 \epsilon_b \frac{\epsilon_a - \epsilon_b}{\epsilon_a + 2\epsilon_b} \vec{E} \tag{2.1}$$

Where ϵ_b is the dielectric constant of the liquid, ϵ_a is the dielectric constant of the microsphere, and r is the radius of the microsphere.

The gradient force is dependent on the dipole moment. Using equation 2.1, we get: [6, 8]

$$F = (\vec{p} \cdot \vec{\nabla})\vec{E} = (4\pi r^3 \epsilon_b \frac{\epsilon_a - \epsilon_b}{\epsilon_a + 2\epsilon_b} \vec{E} \cdot \nabla)\vec{E} \tag{2.2}$$

Therefore, the potential energy of a dielectric microsphere suspended in a dielectric liquid is shown to be:[6, 8]

$$U = -\frac{1}{2}(4\pi r^3 \epsilon_b \frac{\epsilon_a - \epsilon_b}{\epsilon_a + 2\epsilon_b} \vec{E}^2 \tag{2.3}$$

If $\epsilon_a > \epsilon_b$, then the energy will be at a minimum when the electric field is at a maximum. The microsphere moves towards the position where its energy is at a minimum, the electric field maximum. If $\epsilon_a < \epsilon_b$, then the microsphere moves to the electric field minimum.

2.2 Microstrip Theory

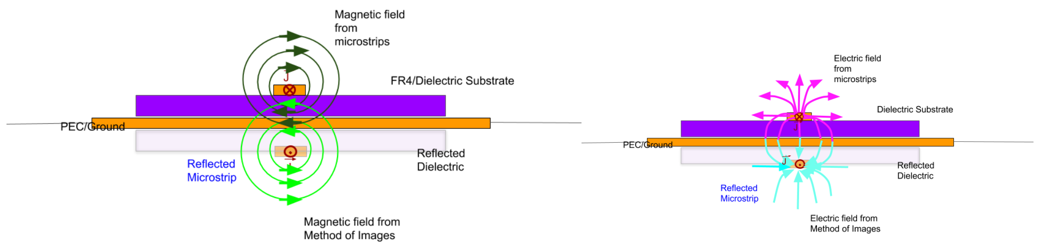

Figure 2.1: The transmission line consists of a trace (orange), dielectric substrate (purple), and a ground plane (orange). The alternating current generates a magnetic field, as seen in the left figure. The magnetic field is represented by the green arrows. The figure on the right shows the corresponding electric field, represented by the pink and blue arrows. Because of the presence of the ground plane, method of images is necessary to find the electromagnetic fields. The fields from method of images is represented by the light green arrows in the left figure and the blue arrows in the right figure.

Microstrips are strips of perfect electric conducting material separated from a ground plane by a dielectric layer. Two of the most popular dielectric substances are FR4 and AlN. Microstrips were developed to propagate an alternating current with a frequency in the microwave range. In the simulations in this paper, the frequencies of the microwaves used varied from 6.8 GHz to 17 GHz, with most simulations running at 6.8GHz, because it corresponds to the hyperfine splitting frequency of rubidium-87 for which the lab has many microwave amplifiers. When the current produced by these microwaves runs through a wire, it creates a magnetic field as shown by the green arrows in figure 4.2. The magnetic field $\vec{B}$ is related to the current I by:

$$\oint \vec{B} \cdot \vec{dl} = \mu_0 I \tag{2.4}$$

From Faradays law, the electric field is related to the magnetic field by:

$$\vec{\nabla} \times \vec{E} = -\frac{d\vec{B}}{dt} \tag{2.5}$$

These equations show that the electric field is dependent on the change of the magnetic field with respect to time. The change in the magnetic field with respect to time is dependent on the change in current with respect to time. Therefore, by sending an alternating current through a microstrip configuration, local magnetic fields and electric fields are created.

In a transmission line, such as a microstrip, the the voltage and the current are related through the characteristic impedance Z of the transmission line. The characteristic frequency is:

$$Z = \frac{V(x,t)}{I(x,t)} \tag{2.6}$$

The characteristic impedance is dependent on the geometry of the transmission line and the properties of the dielectric. [13]. By adjusting the height of the dielectric substrate and the width of the trace, the characteristic impedance can be set to the same impedance of a voltage source and a load attached to the microstrip, preventing current reflections. For example, when a microstrip has the properties of table 2.1 the characteristic impedance of the microstrip is 50 Ω.

All of the voltage sources and loads in this paper will have an impedance of 50 Ω, therefore the characteristic impedance of the microstrips in these simulations is designed to be 50 Ω.

Dielectric Material	Dielectric Constant	Thickness of Substrate	Width of Microstrip for Characteristic Frequency	Characteristic Impedance
AlN	8.9	50μm	55μm	50 Ω

Table 2.1: Example of microstrip parameters for an atom chip based on a AlN dielectric substrate.

2.3 Introduction to Feko

The electromagnetic fields in this thesis are obtained via using the commercial software FEKO. FEKO primarily uses the method of moments to solve for Maxwells equations. FEKO software consists of two packages. The first, CADFEKO, is used to construct and simulate a model. The second, POSTFEKO is used to analyze the plot.

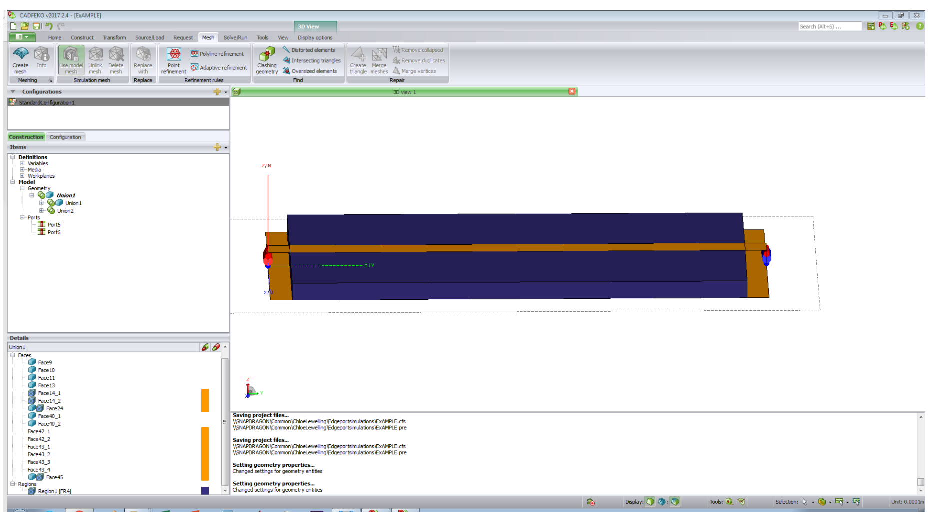

Figure 2.2: An example of a microstrip in CADFEKO. This microstrip consists of the ground plane (the bottom orange rectangle), the substrate (the purple cuboid), and the trace (the top orange rectangle). The edgeports are on both sides of the microstrip and are indicated by a red-blue element.

To simulate a microstrip in FEKO, first a large rectangle is created along the x=0 plane. This rectangle is the ground plane. The material of the ground plane should be PEC, perfect electric conductor. Next, a cuboid region is constructed on top of the plane such that cuboid base is smaller than the rectangle ground plane. This cuboid region is the substrate. The material of this region should be a dielectric material, usually FR4 or AlN. A small rectangle, the microstrip, is constructed so that it is on the same plane as the top face of the cuboid. The rectangle should overhangs the cuboid, as shown in figure 2.2. The width of this rectangle will be dependent on the thickness of the substrate and the material of the substrate. The width is chosen so that the characteristic frequency of the microstip is Z=50Ω. The material of the microstrip should be PEC. Two more rectangles are created, such that they are perpendicular to the microstrip and the ground plane, connecting the edges of the microstrips to the ground plane. These rectangles should be PEC. Next, these rectangles are split at the plane z= half the thickness of the substrate. All constructed elements, the rectangles and the cuboids are unioned. Next, two "edgeports" are added to the two split rectangles, such that the negative face of these edgeports borders the ground plane and the positive face borders the microstrip trace. Voltage sources and loads can be added to these edgeports. Near fields can be requested. The simulation must be meshed before it is run. After it is run, the results are analyzed in POSTFEKO.

2.4 Microstrip Design for Prototyping Boards

The output impedance of our microwave sources is 50 Ω, so the desired characteristic impedance of the microstrip is Z=50Ω. The characteristic frequency of a microstip is dependent on the substrate material, the substrate thickness, and the width of the microstrip. The thickness and the material of the substrate is modelled after commercially available prototype boards, so the width of the microstrip is adjusted to adjust the characteristic frequency. A single microstrip model with a voltage source, $V = 1$ V, $f = 6.8$ GHz, and Z=50 Ω, and a 50 Ω load was constructed for both the FR4 and the AlN prototype board dielectrics. The width of the microstrip was varied to determine at which trace width, the AlN reflection coefficient was at a minimum. The results are in Table 2.2.The prototypeing board-based microstrips are well suited for experiments to trap and manipulate microspheres using microwave "tweezers".

Dielectric Material	Dielectric Constant	Thickness of Substrate	Width of Trace for Characteristic Frequency	Reflection Coefficient
FR4	4.4	0.4mm	0.624mm	0.0785
AlN	8.9	1mm	0.905mm	0.0016

Table 2.2: Model Parameters for Z=50 ω microstrip transmission line base on two commercially available prototyping board.

2.5 Two Strand Trap

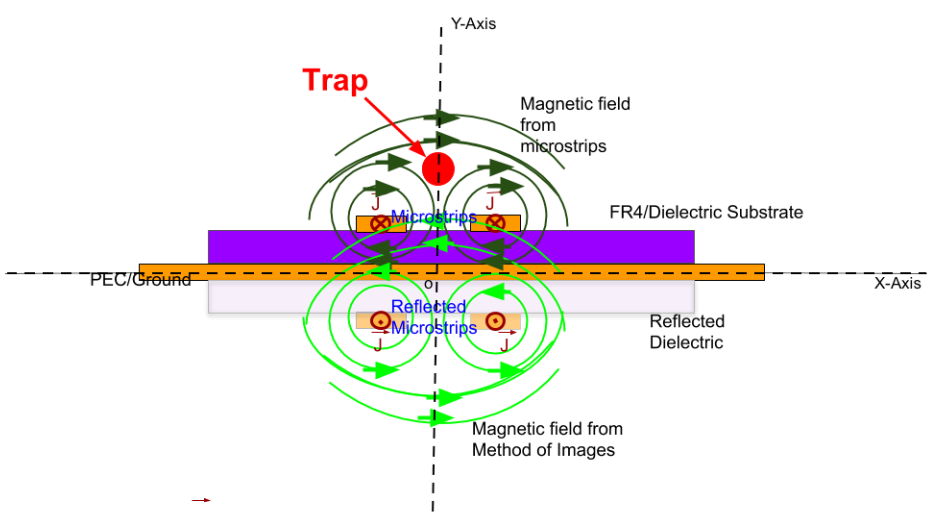

Figure 2.3: Method of images shows that the magnetic field minimum should occur above the microstrip. The location of the magnetic field minimum is indicated by the red circle.

In the two strand trap, a current runs through two parallel microstrips, creating a magnetic field. Treating these microstrips as infinitely long wires, the magnetic field of each microstrip is found by the following:

$$B = \frac{\mu_0 I}{2\pi r} \tag{2.7}$$

, where B is the magnetic field, I is the current, and r is the distance from the wire. The direction of the magnetic field of these microstrips, with a current into the page, will be clockwise due to the right hand rule.

Because of the ground plane and the dielectric, method of images is necessary to obtain the magnetic field for the full microstrip system. This means that the magnetic field above the ground plane has an additional counterclockwise component as seen in Figure 2.3. While the magnetic fields cancel in the $\hat{x}$-direction at $y = 0$, the counterclockwise component of the magnetic field from the image currents is not cancelled in the plane of the microstrips. As seen in figure 2.3, this component will be cancelled above the microstrips by the clockwise component of the magnetic field. Therefore the expected magnetic field minimum should be halfway between the two microstrips and above the dielectric substrate. The electric field minimum is in the same location.

2.6 Three Strand Trap

In the “three strand trap configuration, three currents in phase with each other run through three parallel traces. By the same logic for the two strand trap, the three strand trap will have magnetic and electric minimums between each of the microstrips. If the center trace is adjusted to be 180 degrees out-of-phase with the other two traces, then a single trap is formed above the center trace. In addition, the third microstrip will allow the position of these traps to be moved along the y-axis.

This movement along the y movement will be modelled using the microwave lattice configuration (see section 2.7) as reflections interfere with the simulation. When this trap is constructed, circulators will be used to remove these reflections, but these circulators have not been modelled in FEKO.

2.7 Microwave Lattice

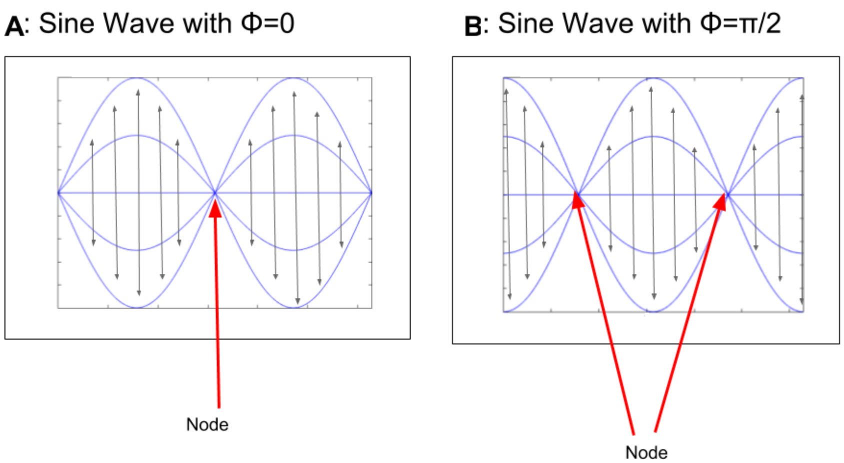

Figure 2.4: The position of the nodes of a sine wave is changed from graph A to graph B by changing the phase of the sine wave.

A standing wave is a wave that does not move along the microstrip propagation axis, but instead oscillates up and down so that its crests and troughs stay in the same position. A standing wave is created by directing two identical traveling waves at each other. In the microwave lattice simulation, two waves are sent in opposite directions, creating a standing wave. As illustrated in figure 2.4, a standing waves has several nodes, or positions where the wave amplitude is always zero. The position of these nodes can be changed by changing the relative phase between the microwaves directed at each other. At the node of the standing wave, there is be an electric field minimum. The position of this electric field minimum can be adjusted by changing the phase of one of the microwave sources. Therefore, by changing the phase of a voltage source, a trapped atom or microsphere can be moved along the microstrip axis.

2.8 Disks

Earnshaws theorem states that for electrostatic and magnetostatic systems, there are no magnetic field or electric field maximums in charge and current-free locations. This derivation relies on:

$$\vec{\nabla} \cdot \vec{E} = 0 \tag{2.8}$$

,

$$\vec{\nabla} \cdot \vec{B} = 0 \tag{2.9}$$

,

However, in the microwave spectrum:

$$\vec{\nabla} \times \vec{E} = \frac{-\partial \vec{B}}{\partial t} \tag{2.10}$$

$$\vec{\nabla} \times \vec{B} = \mu_0 \vec{J} + \mu_0 \epsilon_0 \frac{\partial \vec{E}}{\partial t} \tag{2.11}$$

In the case of the disks, a parallel plate capacitor, the current between them is zero ($\vec{J} = 0$). Therefore:

$$\vec{\nabla} \times \vec{B} = +\mu_0 \epsilon_0 \frac{\partial \vec{E}}{\partial t} \tag{2.12}$$

Consequently, these equations may allow for local electric field and magnetic field maximums in the microwave domain.

In the “disks” configuration simulations, two parallel disks are connected to a voltage source with $V = 1V$ and a frequency of 6.8 GHz. The disks each have a radius of 2 cm and are separated by a distance of 1 cm. A current flows through the circuit, causing the two parallel plates to act as a capacitor. Such a capacitor attached to an AC source with a microwave frequency has a larger electric field towards the center of the disks than towards their edges as seen below: Therefore, there should be a local

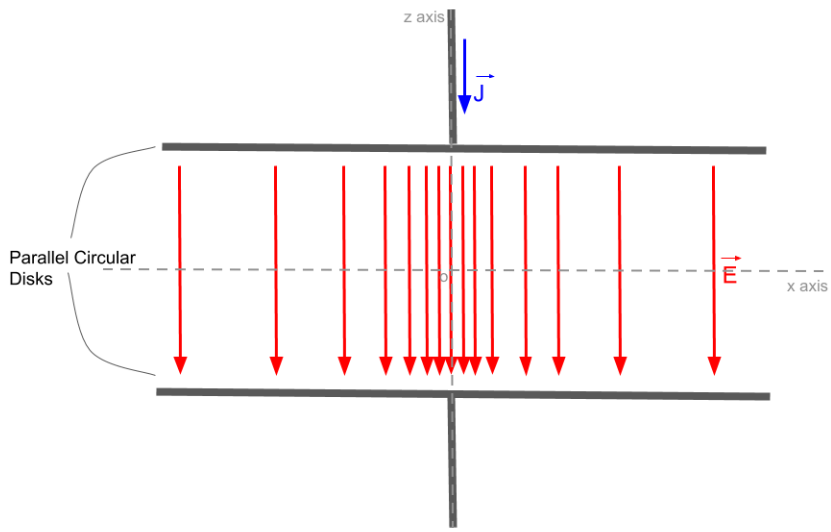

Figure 2.5: Side view of two parallel circular disks. When a microwave current flows through the the circuit, they act as a capacitor with a larger electric field at the center of the disks than at the edges.

electric minimum in the parallel plane halfway between these two disk plates.

2.9 Semi-Spheres

In the semi-spheres geometry, two semi-spheres with a radius 1 cm are separated by a distance of 0.5 cm. When an AC current flows through one of the spheres, it induces a displacement current between the two hemispheres. The spherical capacitor was attached to a voltage source via long wires, and placed in a cubical spherical faraday cage to prevent the electric fields of the wires from affecting the electric field inside the sphere.

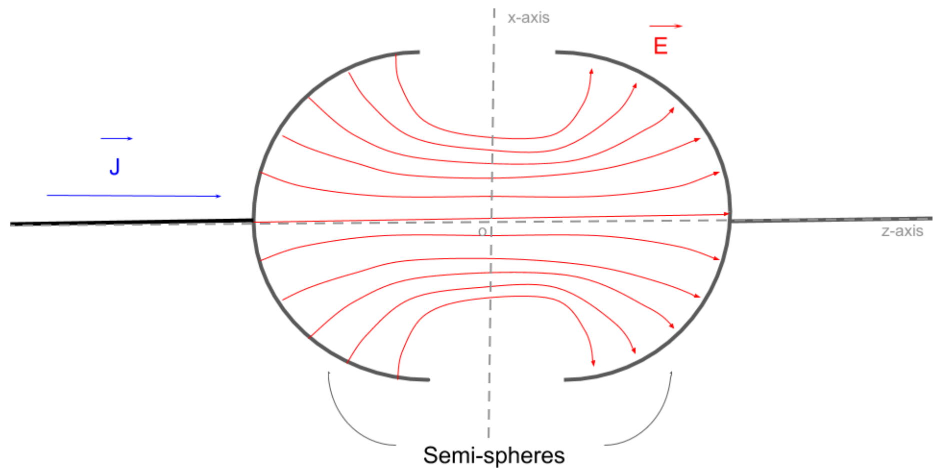

Figure 2.6: A look at the spherical configuration in the x-z planes. The configuration acts as a capacitor, creating an electric field that is greater in the center between the two semi-spheres than near their edges.

As shown in figure 2.6, since the electric field must be perpendicular to the surface of the semi-sphere capacitor, the electric field lines are more compact, (i.e. “focues”) in the center of the capacitor, leading there to a be a local electric field maximum in the x-z and y-z planes. Similar to the case of the two parallel disks, the electric field towards the edges of a capacitor are smaller than the electric fields originating from the center of a capacitor leading there to be a local electric maximum in the x-y direction. Therefore, there is an electric maximum between the two semi-spheres.

2.10 Planar Semi-Circles

The microstrips on the outside of the two half circles induce a current in the half circles, creating a capacitance between them. Using the logic from the sphere and disk configurations, there should exist an electric field maximum in the x-y plane. The two strand trap that surrounds this circle is necessary to push the electric field maximum above the plane, but the mechanism that causes this is unknown. The model for this simulation is in section 4.3.

Chapter 3

Electromagnetic Field Minimums

3.1 Two Strand Trap

3.1.1 Model

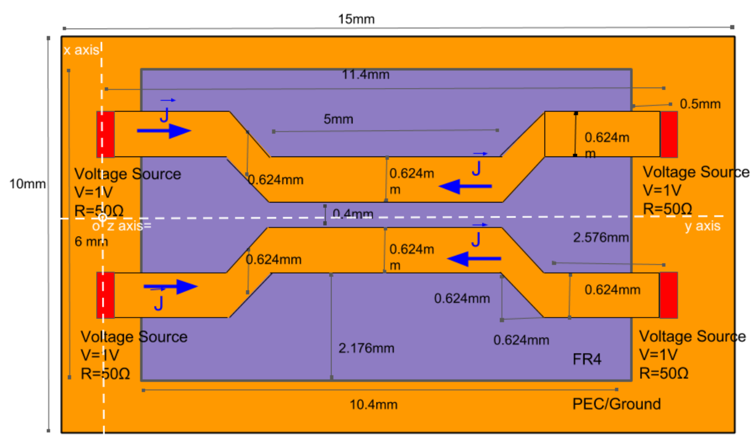

Figure 3.1: Two microstrips which are farther apart at the ends than at the center have voltage source on both ends of the microstrips to create a trap along the y-axis.

The two strand trap is modelled using two microstrips with the dimensions seen in figure 3.1. Voltage sources with V=1 V, R=50 Ω, and frequency f=6.8GHz are attached to either end of both microstrips. Two near fields are simulated from z=1.4 mm to z=10.4 mm. The first near field, Nearfield1 is located between x=-3 mm and x=3 mm at y=5.7 mm. The second near field, Nearfield2 is located between $y = 0$

mm and y=11.4mm at x=0mm. These Nearfields are processed in postfeko to locate an electric field minimum.

3.1.2 Results

The goal of this simulation was to verify and characterize the local electric field minimum (See figure 3.2) above the microstrips.

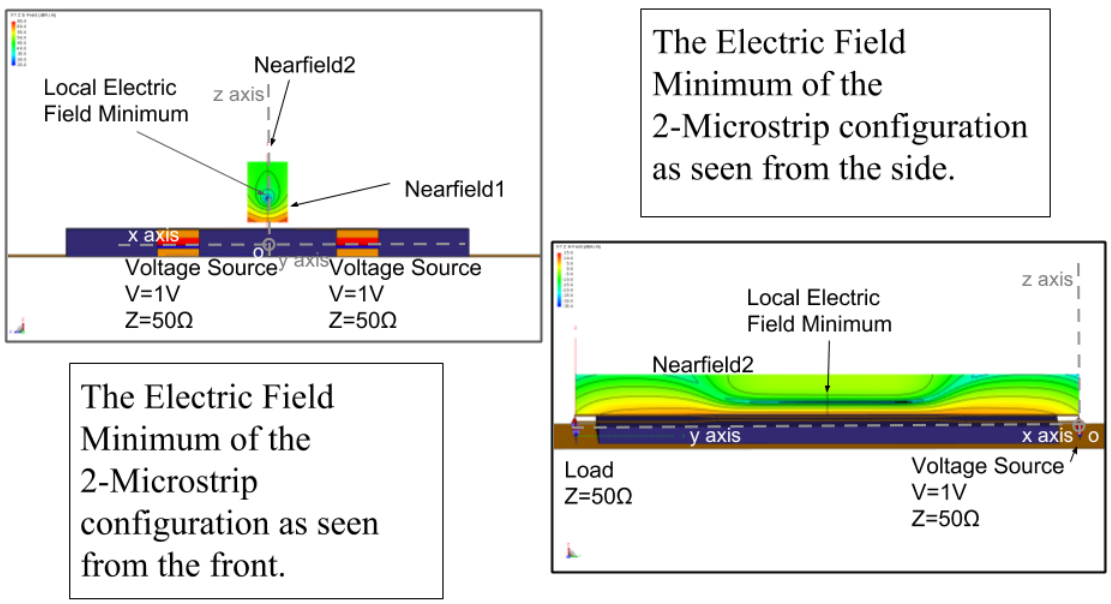

Figure 3.2: The near fields of the two strand Configuration show that there is a local electric field minimum.

As shown in figures 3.3a and 3.3b, the magnetic field minimum occurs halfway between and 0.367mm above the microstrips at $x = 0$mm and $z = 0.767$mm. This magnetic field minimum can potentially be used as an atom trap in future experiments.

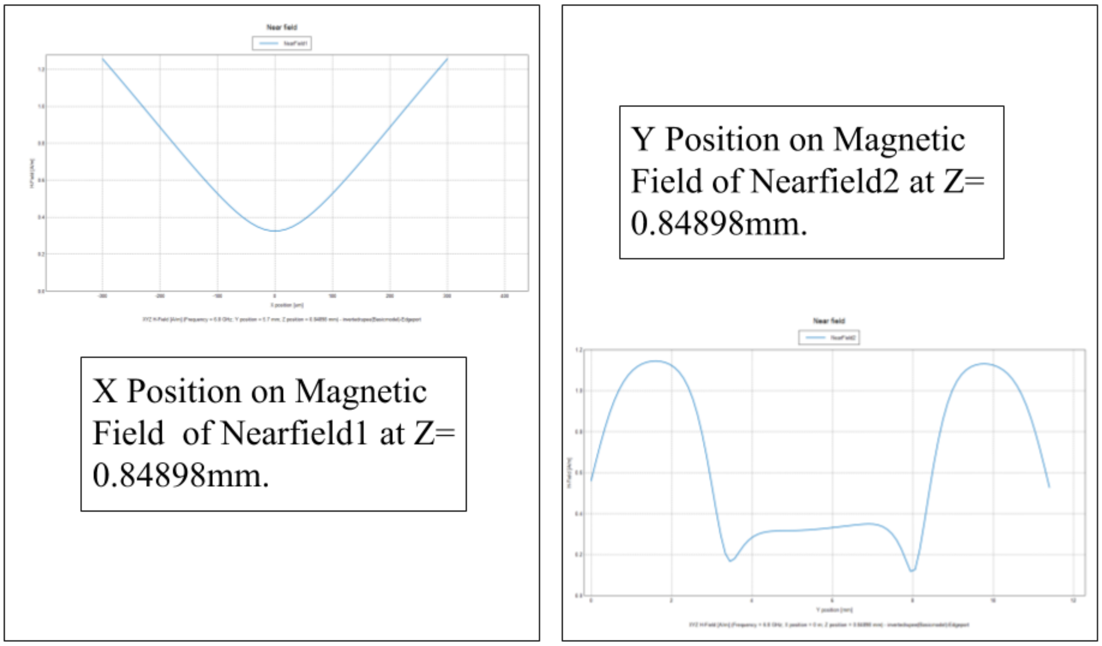

(a) The graphs of near fields of the two strand Configuration show that there is a local electric minimum in the x-y plane.

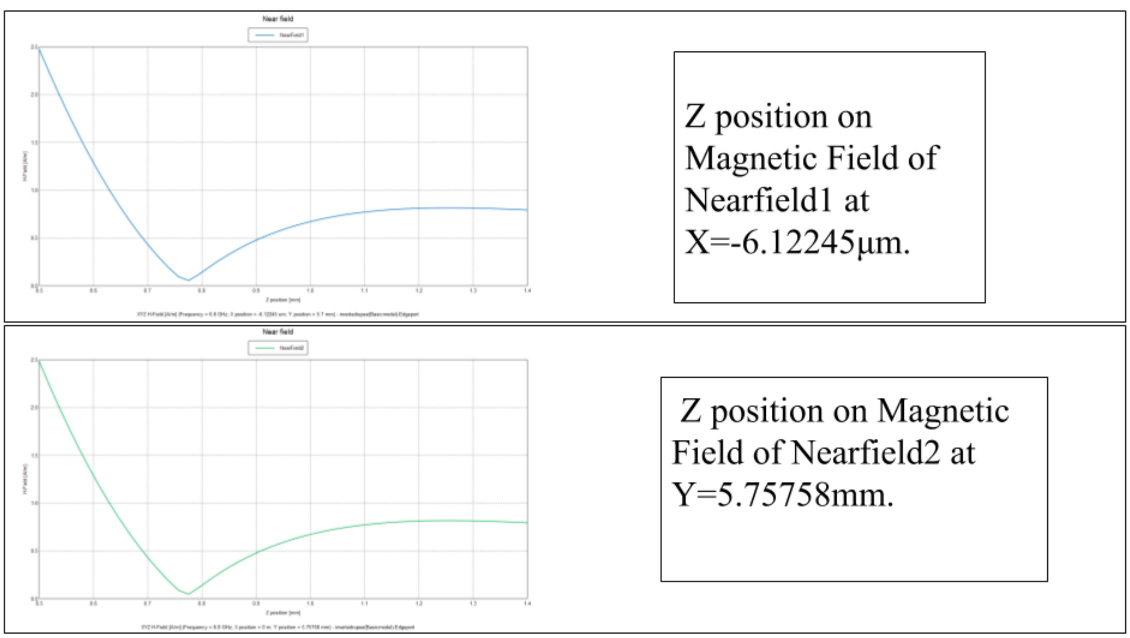

(b) The graphs of near fields of the two strand configuration show that there is a local magnetic minimum along the Z-axis.

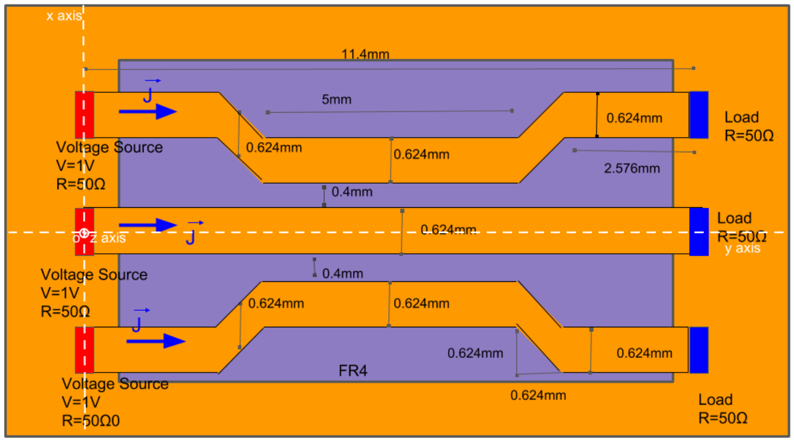

Figure 3.4: In the three strand model, a third microstrip is inserted between the two microstrips of the two strand trap.

3.2 Three Strand Trap

3.2.1 Model

The three strand configuration consists of three parallel microstrips with the dimensions as shown in figure 3.4, are attached to a voltage source, V=1 V, f=6.8 GHz, and $Z_{out} = 50\ \Omega$, and a load, R=50 Ω. Three near fields are modeled between z=0.4 mm and Z=20 mm. Nearfield1 is from x=-19.6 mm to x=19.6 mm at y=5.7 mm. Nearfield2 and Nearfield3 run from y=0 mm to y=11.4 mm. Nearfield2 and Nearfield3 are located at x=7.6 mm and x=-7.6 mm respectively. These fields are processed in POSTFEKO to find the electric field minima.

3.2.2 Results

The goal of the three strand microstrip is to create and characterize two electric field minima above the microstrips. Figure 3.5 shows the two electric minima generated by the simulations.

Figure 3.6 show that electric field minimums occur at $z = 0.9$ mm and $y = 5.7$

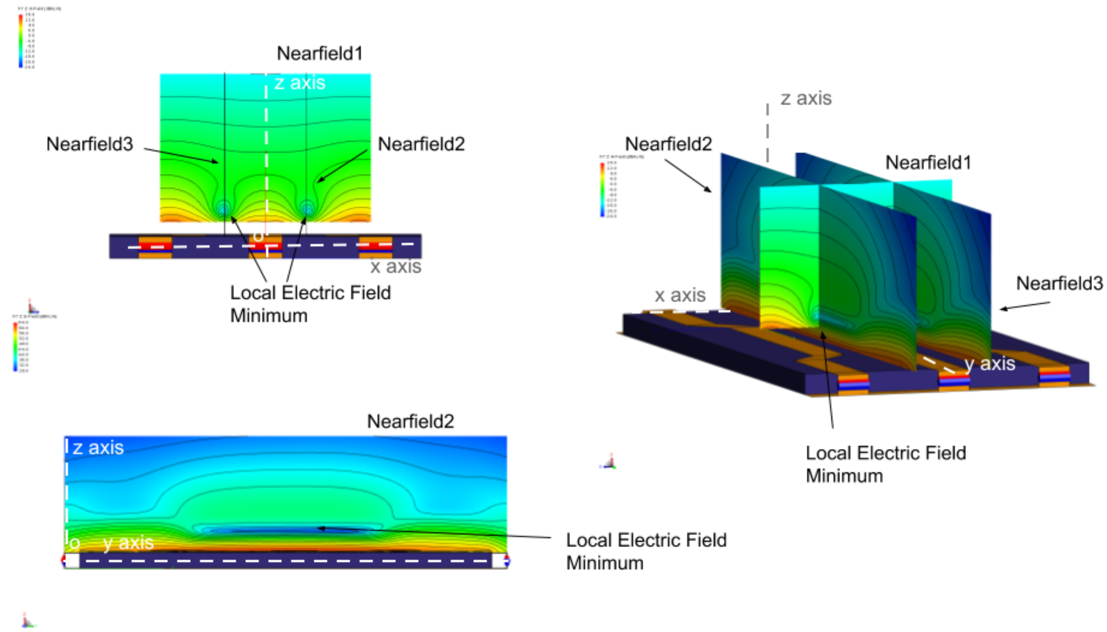

Figure 3.5: The near fields of the three strand configuration show that there is a local electric minimum.

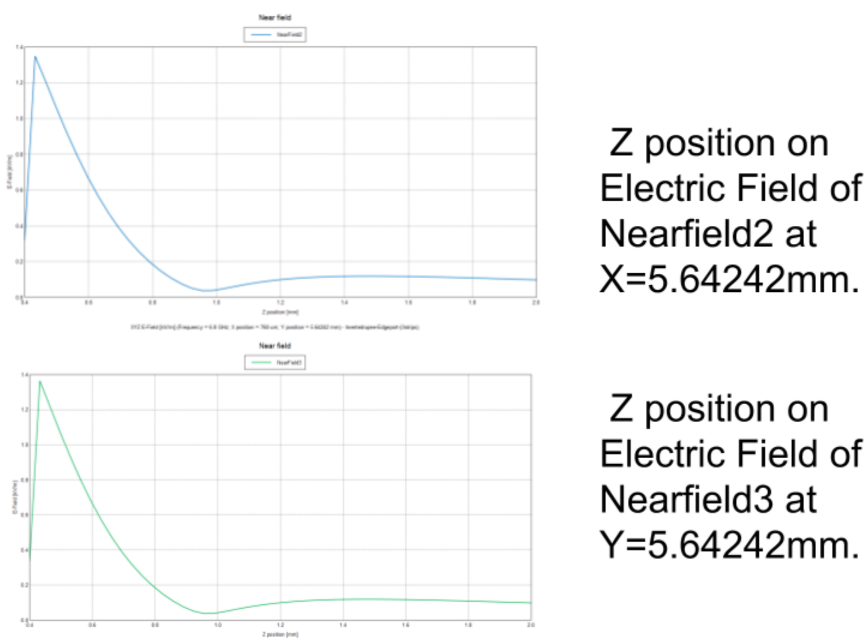

Figure 3.6: The graphs of near fields of the two strand configuration show that there is a local electric minimum along the Z-axis.

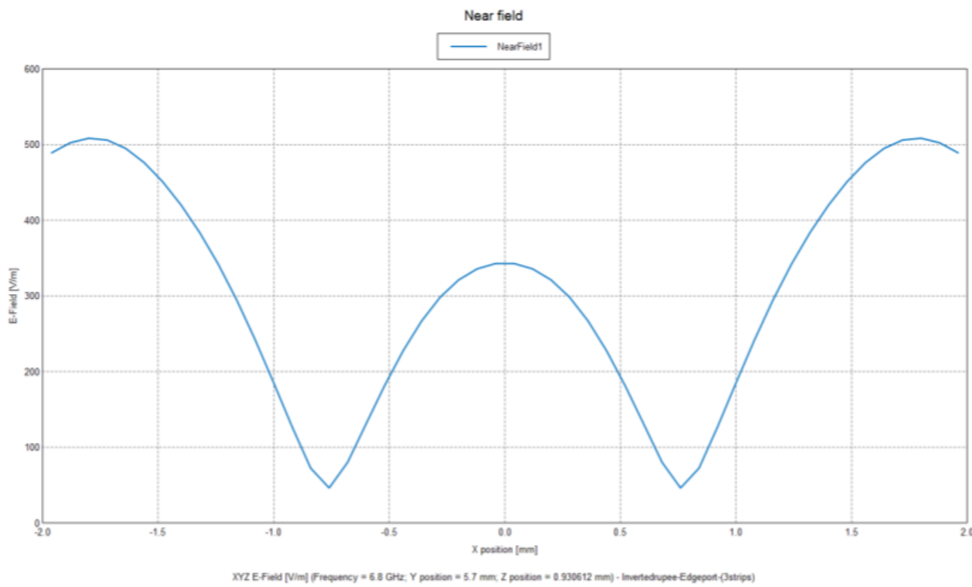

Figure 3.7: This Graph shows that there are two electric minimums in the x-z plane

mm. One minimum occurs at $x = -0.7$ mm. The other minimum occurs at $x = 0.7$ mm. These electric field minimums are above the microstrips and occur in all three dimensions. Each of the minima occurs halfway between two microstrips.

3.3 Microwave Lattice

3.3.1 Model

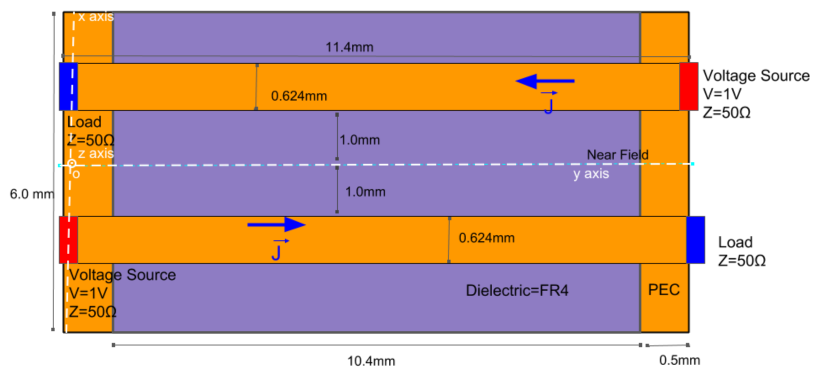

Figure 3.8: Test model for simulating the microwave lattice. This configuration creates a standing wave in the perpendicular plane halfway between the two microstrips

The microwave lattice configuration is modelled using the geometry in figure 3.8. A voltage source, $V = 1$ V, $f = 6.8$ GHz, and $Z = 50\ \Omega$, is attached to both microstrips at opposite ends of the microstrips. Loads with $Z = 50\ \Omega$ are attached to the other end of the microstrip. A near field, Nearfield1 is located at $x = 0$ mm, and from y=0 mm to y=11.4 mm. The local electric field minimum is identified using POSTFEKO. The simulation is run again with a varying phase for voltage source 1, and the location of the electric field minimum is correlated with this phase.

3.3.2 Results

The objective of the microwave lattice simulations is to show that the electric field minimum can be moved by changing the phase of one of the voltage sources.

Figures 3.9 and 3.10 show that when $\phi = 0°$, the electric field minimum is located at y=5.7 mm. The figures also show that when $\phi = -30°$, $\phi = -60°$, $\phi = -90°$,

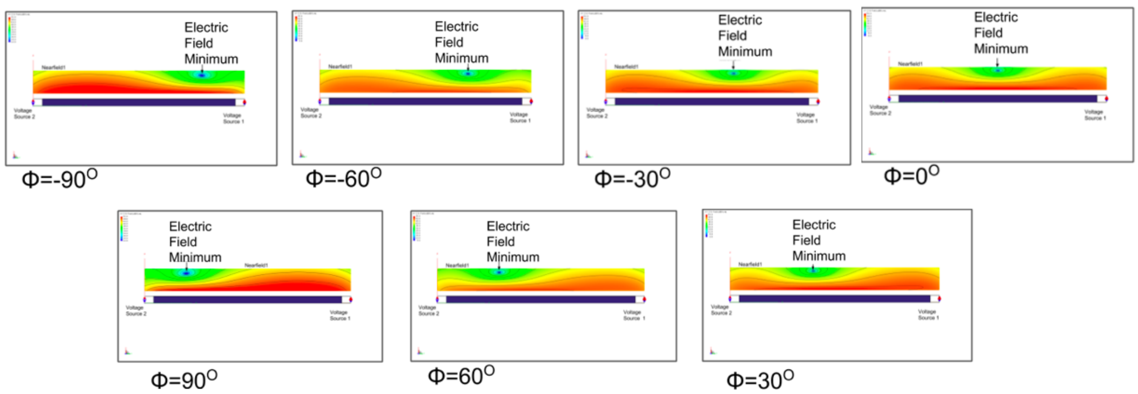

Figure 3.9: The position of the electric field minimum can be adjusted by changing the phase of voltage source 1.

$\phi = 30°$, $\phi = 60°$, and $\phi = 90°$, the electric fields are located at $y = 6.7$ mm. $y = 8$ mm, $y = 9$ mm, $y = 4.6$ mm, $y = 3.7$ mm, and $y = 2.2$ mm respectively. This shows that once microspheres are trapped in an electric field minimum, they can be transported by slowly changing the phase of the voltage source of the lattice. This scheme potentially allows for the transport of trapped atoms.

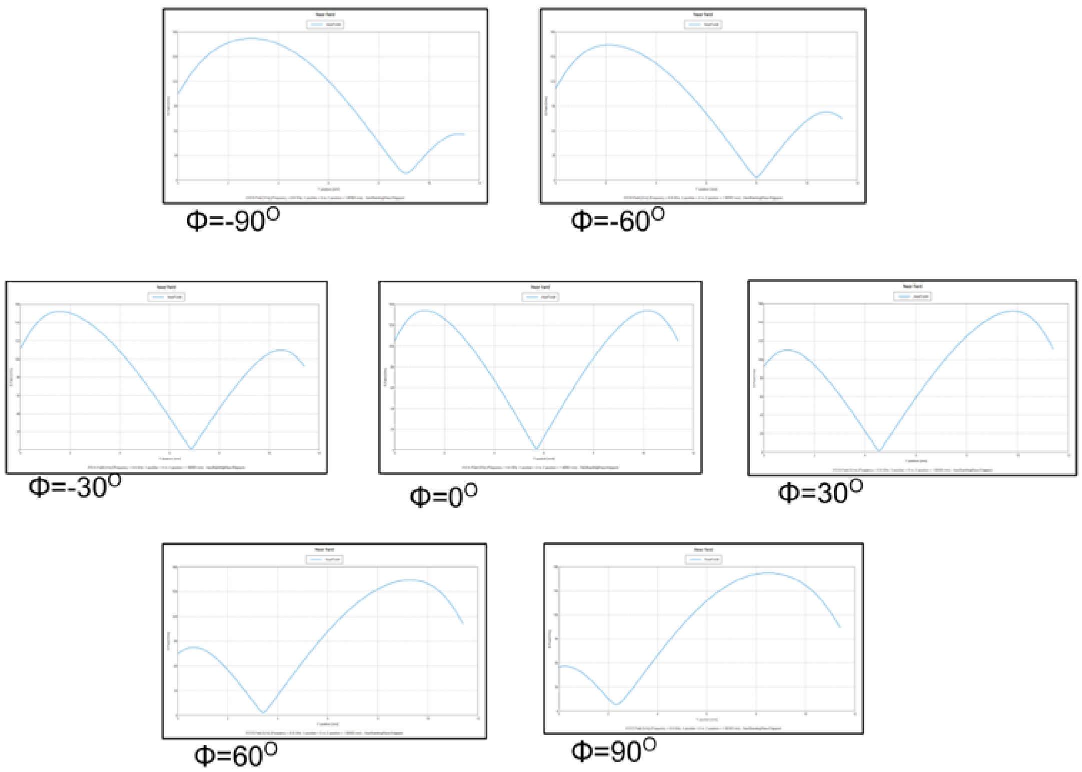

Figure 3.10: The position of the electric field minimum can be adjusted by changing the phase of voltage source 1.

Chapter 4

Electromagnetic Field Maximums

In this chapter, I summarize the results on generating a microwave electric near field maximum.

4.1 Disks

4.1.1 Model

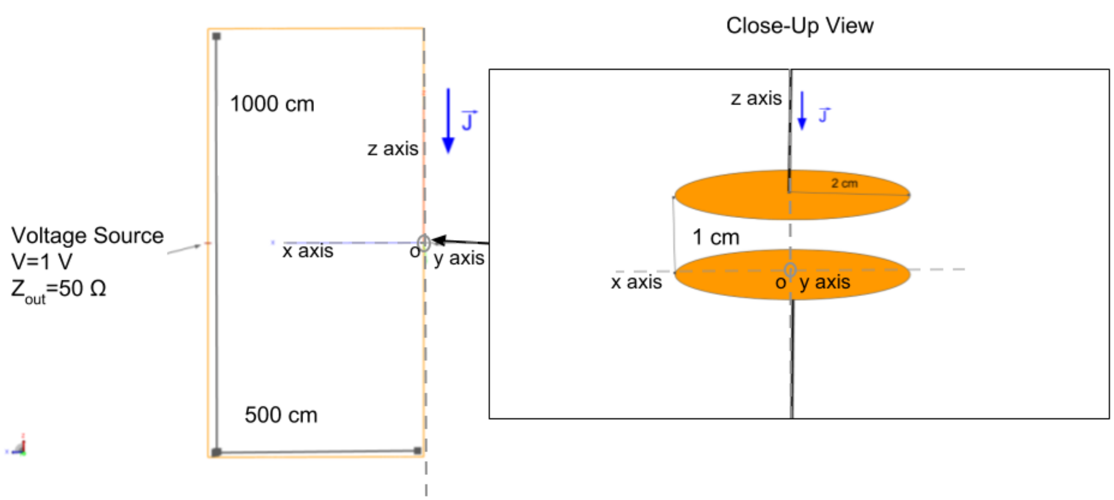

Figure 4.1: The parallel-plate capacitor "disk" model is placed in a large circuit connected to a voltage source with $V = 1$ V, $f = 12$ GHz, and $Z_{out} = 50\ \Omega$.

The disk model consists of two circular parallel plates with a radius of 2 cm that are separated by a distance of 1 cm and attached to a wire circuit. The circuit has corners at (0, 500 cm), (500 cm, 500 cm), (500 cm, -500 cm) and (0, -500 cm). A voltage source with $V = 1$ V, $Z_{out} = 50\ \Omega$, and $f = 12$ GHz is located at (0, 500 cm). The electric fields between the two disks is calculated by FEKO.

4.1.2 Results

The objective of the "disk" configuration simulation is to verify the existence of an electric field maximum in the x-y plane.

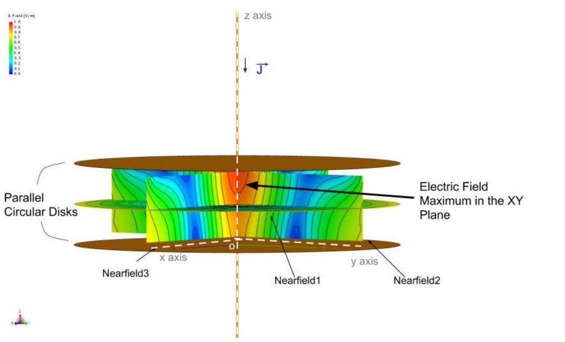

Side view of the electric field between two circular disks that act as a capacitor. The electric field has a local maximum in the xy direction.

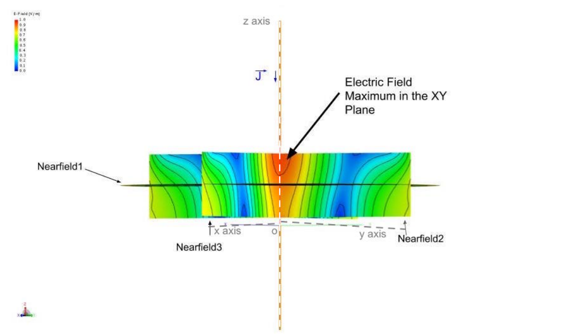

Another view of the electric field between the two disks shows that the electric field maximum occurs at x=0, y=0 in the xy-plane.

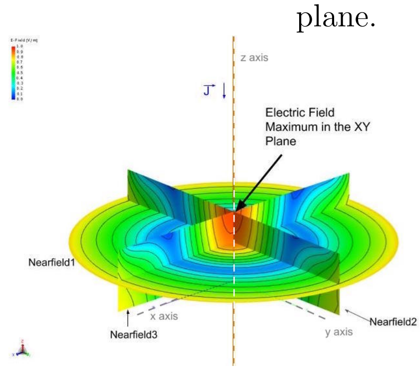

Another side view shows what the electric fields look like when they are not obscured by the disks.

Figure 4.2: Above are the results of the disks configuration simulation. The disks configuration has an electric field minimum in the x-y plane.

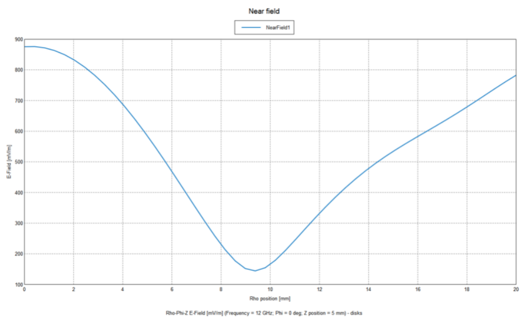

The ρ position on E-Field shows that for Nearfield1 and other fields in the xy-plane, there is a local electric field maximum at ρ=0.

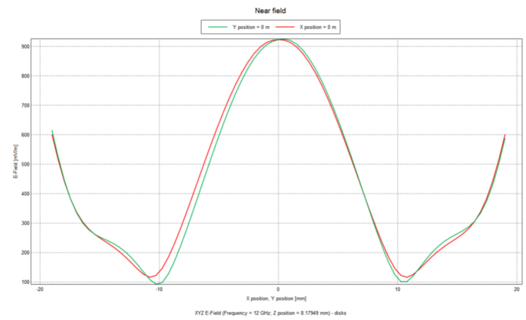

The graphs of x-position on E-field of Nearfield3 and y-position on E-field of Nearfield2 show that there is is an local electric field maximum in the x and y directions at x=0 and y=0 respectively.

Figure 4.3: These graphs show that there is a local electric maximum at x=0, y=0 in the x-y plane.

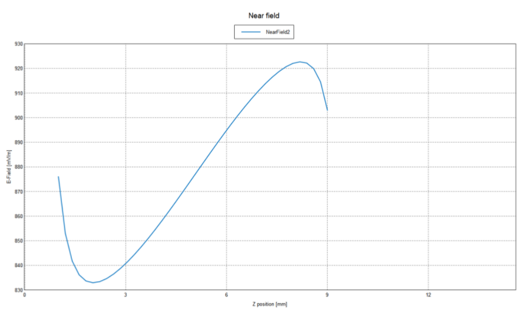

The Graph of Z position on E-Field of Nearfield2 shows that the electric field is largest right next to the top parallel plate.

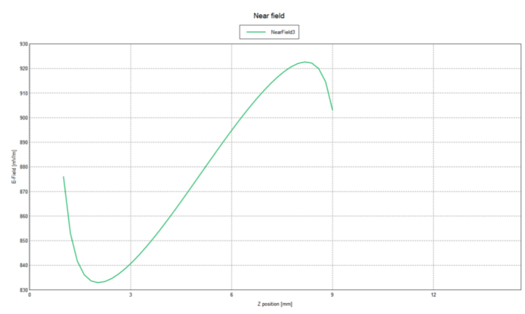

The Graph of Z position on E-Field of Nearfield3 shows that the electric field is largest right next to the top parallel plate.

Figure 4.4: These graphs show that the Electric field is greatest along the z-axis next to the top parallel disk.

As shown in figures 4.3 and 4.4, The parallel disks configuration produced an local electric field maximum at $z = 8.1795$ mm in Nearfield2 and $z = 8.1795$ mm in Nearfield3 and at $\rho = 0$ mm. The electric field is greatest along the z axis next to the the top parallel plate, and the electric field is weakest halfway between the center of the disks and their circumference.

4.2 Two Semi-Spheres

In this model, the disks model is curves as to generate a 3D microwave near field maximum

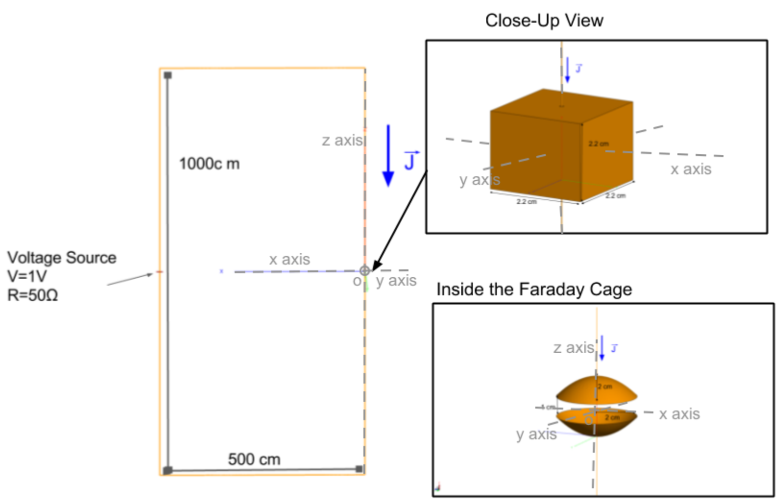

Figure 4.5: The spherical configuration is located in a large circuit attached to a voltage source of $V = 1$V, $R = 50$, and $f = 6.8$GHz. A faraday cage is used to limit the influence of the wires electric field on the electric field inside the sphere.

This model consists of two semi-spheres with a radius 2 cm are separated by a distance of 1 cm. The ends of these semi-spheres are connected to a wire circuit located in the xz plane with corners at (0 cm, 500 cm), (500 cm, 500 cm), (500 cm , -500 cm), and (0 cm, -500 cm). A voltage source of $V = 1V$, $Z_{out} = 50\ \Omega$, and frequency 6.8 GHz is placed at (500 cm, 0 cm). The near fields in the $x = 0$ cm, $y = 0$cm, and $z = 1.5$ cm planes are simulated.

4.2.1 Results

The main goal of the semi-spheres configuration is to determine if a local electric field maximum can be generated along all three axises. There is an electric maximum

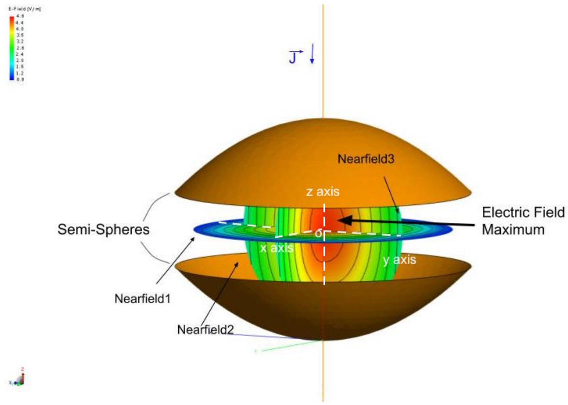

The electric field between two semi sphere has a maximum between the origins of the two semi-spheres.

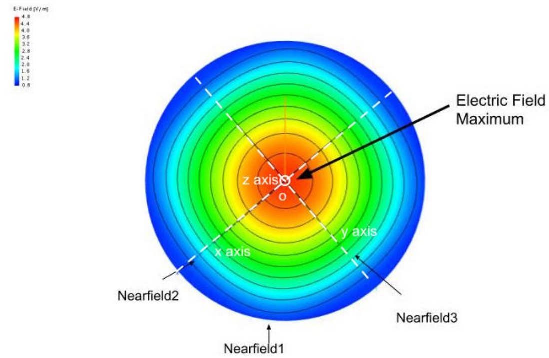

The electric field and its maximum as seen from above

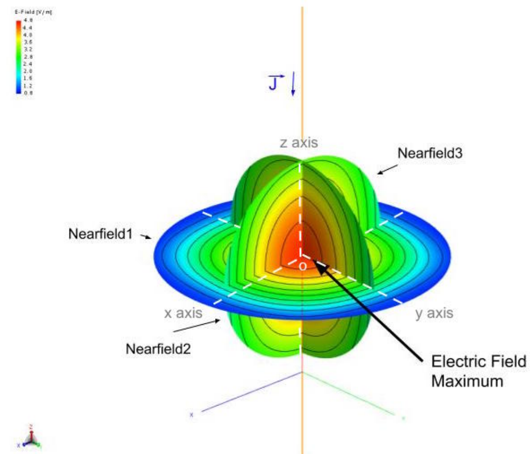

The electric field inside the spheres as seen from the side.

Figure 4.6: These graphs show that the Electric field is greatest along the z-axis next to the top parallel disk.

when $\rho_1 = 0$, $\rho_2 = 0$, and $\rho_3 = 0$. This corresponds to a magnetic minimum at $x = 0$, $y = 0$, and $z = 0$. The electric field is strongest halfway between the semi-spheres and gets weaker as it gets closer to the semi-spheres. This shows that Earnshaw's theorem does not prevent local electric field maxima for microwave electromagnetic near fields.

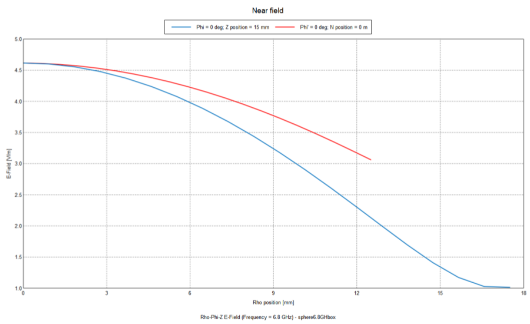

The ρ on E-Field graph for Nearfield1 and Nearfield2 show she electric field has a local maximum when ρ =0mm, at the center of Nearfield1 and Nearfield2.

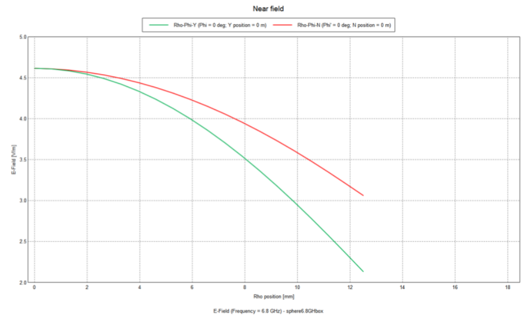

The ρ on E-Field graph for Nearfield2 and Nearfield3 show she electric field has a local maximum when ρ =0mm, at the center of Nearfield2 and Nearfield3.

Figure 4.7: 3D-Neat maximum for the semi-spheres configuration. There is a local electric field maximum in the center of the sphere configuration

4.3 Planar Semi-Circles

This section describes a prototyping board compatible model for creating a microwave electric field maximum.

4.3.1 Model

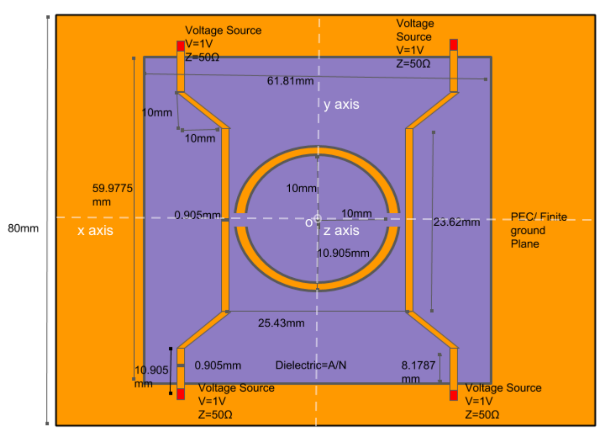

Figure 4.8: Planar Semi-Circles Model. Two semi-circles are surrounded by the two strand configuration.

The model consists of two semicircles with an inner radius of 9mm are separated by 1mm. This geometry is surrounded by the two strand configuration (see section 3.1) and seen in Figure 4.8. Five circular near fields, parallel to the ground plane with a radius 31.7 mm are simulated. Nearfield1_6, Nearfield1_4, Nearfield1_2, Nearfield1_1, and Nearfield1_2 are located at $z = 70$ mm, $z = 65$ mm, $z = 60$ mm, $z = 55$ mm and $z = 50$ mm respectively. Nearfield2 is located at $x = 0$ mm, and between $y = -31.7$ mm and $Y = 31.7$ mm, and between $z = 25$ mm and $z = 10$ mm. Nearfield3 is located at $y = 0$ mm, and between $x = -31.7$ mm and $x = 31.7$ mm, and between $z = 25$ mm and $z = 10$ mm. This configuration is simulated for $f = 17$ GHz. Analysis with POSTFEKO showed an electric field maximum above the substrate.

4.3.2 Results

The goal of the planar semi-circles configuration is to create a local electric field maximum using microstrips. Figures 4.9 and 4.10 show that there is a local electric maximum at $Z = 0$ mm, $Y = 0$ mm, and $Z = 52$ mm. This can potentially be used to trap dielectric microspheres that are high field seekers. Notably, the reflection coefficient measurement in the voltages sources was large. This is a result of modeling the voltage source using edgeports in FEKO. When two voltage sources are added to opposite ends of the microstrip, it creates a large reflection coefficient. It should be noted that it is unclear if the observed maximum is a near field or far field maximum.

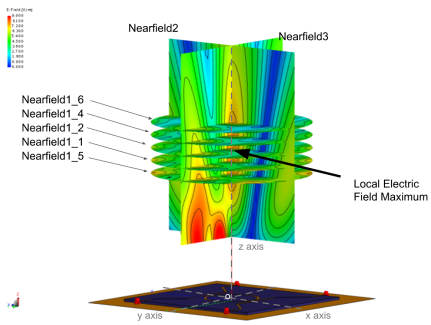

The electric field as seen from an angle.

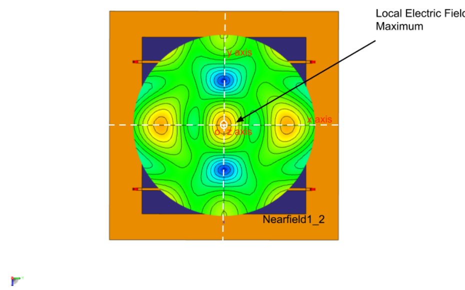

The electric field as seen from above.

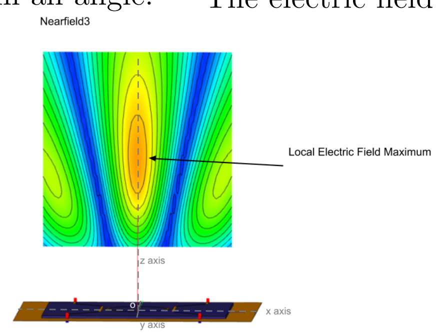

The electric field as seen from the side.

Figure 4.9: There is a local electric field maximum above the center of the configuration.

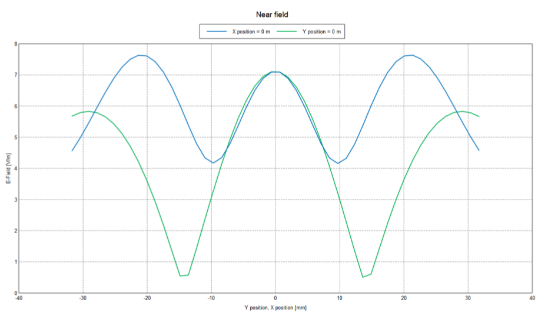

The x-position and y-position on the E-field for Nearfield2 and Nearfield3

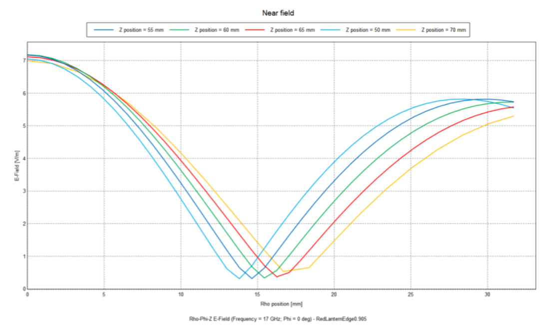

The ρ-position on the E-field for Nearfield1$_6$, Nearfield1$_4$, Nearfield1$_2$,Nearfield1$_1$, and Nearfield1$_5$

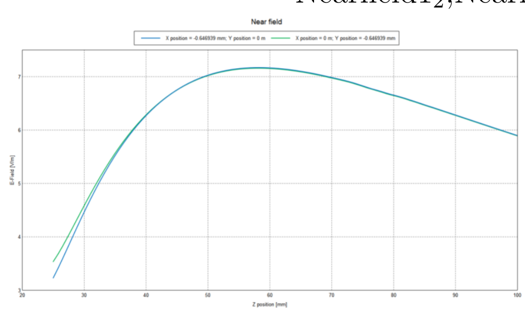

The z-position on the E-field for Nearfield2 and Nearfield3

Figure 4.10:]
There is a local electric field maximum above the center of the configuration.

Chapter 5

Conclusion

Electromagnetic field minimums and maximums were simulated using FEKO. These field minimums and maximums can be used to create electromagnetic microwave traps. More specifically, this thesis research showed that:

- The "two strand trap" configuration created a magnetic field minimum.
- The "three strand trap" configuration created two magnetic field minimums.
- The "microwave lattice" scheme created an electric field minimum along the microwave trace axis who position can be changed by adjusting the phase of the microwave sources the generate the lattice.
- The parallel plate capacitor "disks" configuration created an electric field maximum in the x-y plane
- The "semi-sphere" model created an electric field maximum in all three directions
- The "planar semi-circle" model created an electric field maximum above the planar substrate.

In the future, using the microwave lattice, the three strand configuration will be built and tested for microspheres. If it successfully traps and moves microspheres, it may be used as an atom chip to perform atom interferometry. The planar semi-circles diagram created an electric maximum using planar geometry and microstrips. Some of these geometries can be built on prototyping boards. These prototyping boards can be submerged in a dielectric liquid, and tested to see if they can successfully trap dielectric spheres.

Bibliography

[1] Brugger, K., Krger, Luo, Wildermuth, Gimpel, Klein, . . . Schmiedmayer. (2005). Two-wire guides and traps with vertical bias fields on atom chips. Physical Review. A : Atomic, Molecular, and Optical Physics, 72(2), 023607.

[2] Davis, T. (2002). 2D magnetic traps for ultra-cold atoms: A simple theory using complex numbers. The European Physical Journal., 18(1), 27-36.

[3] De Vlaminck, I., & Dekker, C. (2012). Recent Advances in Magnetic Tweezers. Annual Review of Biophysics., 41(1), $453 - 472$.

[4] Dervos, C., Paraskevas, Skafidas, & Vassiliou. (2005). Dielectric characterization of power transformer oils as a diagnostic life prediction method. IEEE Electrical Insulation Magazine a Publication of the IEEE Electrical Insulation Society., 21(1), 11-19.

[5] EM Software & Systems-S.A. (Pty) Ltd. (2014). Feko: User Manual Retrieved from https://altairuniversity.com/wp-content/uploads/2015/03/UserManual.pdf

[6] Griffiths, David J. (2014) Electric Fields in Matter. Pearson Introduction to Electrodynamics. 4th e d. (pp. 167-209) Print.

[7] Gustavson, T., Chikkatur, A., Leanhardt, A., Grlitz, A., Gupta, S., Pritchard, D., & Ketterle, W. (2001). Transport of Bose-Einstein Condensates with Optical Tweezers. Physical Review Letters, 88(2), 020401.

[8] Lu, Z., Murakowski, J., Schuetz, C., Shi, S., Schneider, G., Samluk, J., & Prather, D. (2006). Perfect lens makes a perfect trap. Optics Express, 14(6), 2228.

[9] Recent News (2017, March 10). Retrieved April 20, 2018, from `http://saaubi.people.wm.edu/ResearchGroup/News/news.html`

[10] Novotny, L., Bian, R., & Xie, X. (1997). Theory of Nanometric Optical Tweezers. Physical Review Letters, 79(4), 645-648.

[11] Smith, C., & Ray-Sun Chang. (1980). Microstrip Transmission Line with Finite-Width Dielectric. IEEE Transactions on Microwave Theory and Techniques., 28(2), 90-94.

[12] Weinstein, J., & Libbrecht, K. (1995). Microscopic magnetic traps for neutral atoms. Physical Review. A : Atomic, Molecular, and Optical Physics, 52(5), 4004-4009.

[13] Wheeler, H.A. (1965). Transmission-Line Properties of Parallel Strips Separated by a Dielectric Sheet. IEEE Transactions on Microwave Theory and Techniques, 13(2), 172-185. DOI: 10.1109/TMTT.1965.1125962